THE JOURNAL OF PHYSICAL CHEMISTRY C

Article

pubs.acs.org/JPCC

Carbon Support Effects on the Hydrogen Storage Properties of $LiBH_4$ Nanoparticles: A First-Principles Study

Ebrahim Hazrati,*[,†] Geert Brocks,[‡] and Gilles A. de Wijs*[,†]

[†]Institute for Molecules and Materials, Radboud University Nijmegen, Heyendaalseweg 135, 6525 AJ Nijmegen, The Netherlands

[‡]Computational Materials Science, Faculty of Science and Technology and MESA+ Institute for Nanotechnology, University of Twente, P.O. Box 217, 7500 AE, Enschede, The Netherlands

ABSTRACT: $LiBH_4$ nanoparticles confined in nanoporous carbon materials show improved hydrogen storage properties. Using density functional theory calculations, we study how the thermodynamics of the decomposition reactions of $LiBH_4$ nanoparticles is affected by the chemical interactions between the reactant or products and the nanoporous carbon host. We find that the reversible intercalation of Li as one of the reaction products into the graphitic carbon host has a large effect on the reaction enthalpies of small clusters. Explicit calculations show that small $(LiBH_4)_n$, $n \lesssim 12$, clusters decompose at much lower temperatures in the presence of graphite, leading to the formation of intercalated Li. This route becomes unfavorable for larger $(LiBH_4)_n$ clusters, where dehydrogenation leads to the formation of $(LiH)_n$ clusters.

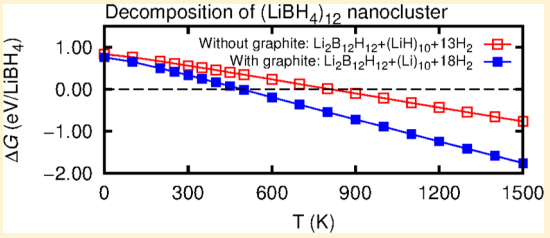

1. INTRODUCTION

The ideal hydrogen storage system should have large gravimetric and volumetric storage capacities, suitable thermodynamic properties, and fast hydrogen absorption and desorption kinetics.[1] As simple (metal)hydrides do not meet these requirements, attention has focused on more complex hydrides in recent years.[2,3] $LiBH_4$ has a high gravimetric capacity of 18.5 wt %, which makes it one of the most interesting complex hydrides for hydrogen storage.[4−9] However, $LiBH_4$ is a relatively stable material that decomposes at a high temperature ($T \gtrsim 400$ °C). Furthermore, rehydrogenation is possible only at extreme conditions with typical values for temperature and pressure of 600 °C and 350 bar H_2. Moreover, the de/rehydrogenation kinetics is slow, which is a common problem in bulk complex hydrides.[5,10−12]

A recently adopted approach that helps to address such problems is nanoconfinement in porous materials.[13−15] For instance, experimental and theoretical studies show that nanoconfinement of $NaAlH_4$ in porous carbon improves the H_2 sorption kinetics and that, somewhat surprisingly, nanoconfinement also alters the decomposition thermodynamics.[16−19] This approach can also be applied to $LiBH_4$. Indeed, improving its sorption properties via nanoconfinement in porous materials has become the focus of much experimental work.[20−31] Faster dehydrogenation kinetics has been reported for $LiBH_4$ infiltrated in carbon aerogels, nanoporous carbon, and nanoporous silica. This is accompanied by a decrease of the dehydrogenation temperature by at least 100 °C. Confinement of $LiBH_4$ in nanoporous carbon also leads to a marked improvement of the reversibility of the hydrogen desorption.

These findings could be the result of changed kinetics, as obviously nanoconfinement puts a limit on the particle size, which will reduce the diffusion distance required for mass transport. Moreover, nanoparticles have a large surface-to-bulk ratio, which is benificial as decomposition reactions are much more likely to occur at the surface than in the interior of a particle.[32,33] It is also possible that the cluster size and the interactions with the host modify the thermodynamics of the reactions.

In a previous work, we studied the stability of $(LiBH_4)_n$ nanoclusters as a function of their size, as well as the stability of a range of possible nanocluster decomposition products.[34] Our findings suggest that, from a thermodynamic point of view, the desorption reactions of unsupported $LiBH_4$ nanoclusters with a diameter larger than ∼2 nm are indistinguishable from those of bulk $LiBH_4$ (i.e., decomposition to $Li_2B_{12}H_{12}$ followed by a second decomposition step to LiH and B). Only for clusters that have a diameter less than ∼1 nm, i.e. $(LiBH_4)_n$ with $n < 12$, is the thermodynamics of the decomposition reaction significantly different. The thermodynamics of small clusters is unfavorable, however, and leads to hydrogen desorption temperatures higher than those of bulk. The reason is that, although $(LiBH_4)_n$ clusters are destabilized with respect to bulk, clusters of possible reaction products are even more destabilized. This means that the improved (de)hydrogenation of nanoconfined $LiBH_4$ observed in experiment cannot be caused by changes in the thermodynamics of the $LiBH_4$ nanoclusters. Such effects could have a kinetic origin or could be due to a chemical interaction between the reactant or products and the host material.

Indeed, such chemical interactions have been observed in NaH, for instance. A recent experiment has shown that the

Received: October 29, 2013
Revised: February 17, 2014
Published: February 18, 2014

   dx.doi.org/10.1021/jp410676b | J. Phys. Chem. C 2014, 118, 5102−5109

improved thermodynamic properties of NaH nanoparticles, compared to those of bulk NaH, are partly due to interactions with the nanoporous carbon host.[35] An increase in the average graphene interlayer spacing distance from 3.35 to 3.54 Å has demonstrated intercalation of Na between the graphene layers.[36] Reversible intercalation of Na into the nanoporous carbon matrix stabilizes Na relative to its metallic phase, which lowers the dehydrogenation enthalpy.[35]

In the case of nanoconfined $LiBH_4$, Li metal is potentially one of the reaction products of dehydrogenation. Intercalation of Li into graphite is a well-characterized process. Graphite can store Li to form Li-graphite with general formula Li_xC_6 ($0 \leq x \leq 1$). The intercalation process is highly reversible, which makes graphitic carbon one of the most commonly used anode materials in rechargeable Li-ion batteries.[37,38] Our calculations give a small activation energy for diffusion of Li atoms on graphene (single-layer graphite) of 0.25 eV,[39] which leads to fast diffusion. A recent experimental study suggests that Li atom diffusion across the graphene planes is the rate-limiting step in Li intercalation into graphite. It reports an even smaller activation energy for diffusion of 0.16 eV, corresponding to a very large diffusion coefficient $D \approx 5 \times 10^{-6}$ cm^2 s^{-1} at room temperature.[40] If $LiBH_4$ is in close contact with the nanoporous carbon host, then during dehydrogenation of $LiBH_4$, Li might intercalate into the carbon material. Indeed, recent in situ X-ray Raman spectroscopy of $LiBH_4$ in porous carbon shows that part of the Li intercalates during dehydrogenation.[41] The studies on Li intercalation show that this process will not result in any additional kinetic barriers regarding the reversibility of $LiBH_4$ (de)hydrogenation.

In this work we study how the thermodynamics of the decomposition reactions of $LiBH_4$ nanoparticles is affected by the chemical interactions of reactant and product particles with the nanoporous carbon host using first-principles density functional theory. The carbon host typically contains domains of regular or irregular stacks of graphene sheets as well as an amorphous fraction and a large number of voids, see ref 15. We use graphite and graphene as model systems to represent the carbon host.[42] In particular, we address the effect of Li intercalation into graphite on the decomposition pathways and reaction enthalpies.

This paper is organized as follows. In Section 2 we describe the computational procedures used. In Section 3.1 we calculate the interaction energies between the reactant/products and graphene. These data are used in Sections 3.2.1 and 3.2.2 to study the decomposition reactions of small and large $(LiBH_4)_n$ nanoclusters, respectively. Section 4 presents a summary and the conclusions.

2. COMPUTATIONAL METHODS

First-principles calculations were performed in the framework of density functional theory (DFT)[43,44] using the Perdew–Burke–Ernzerhof (PBE) generalized gradient approximation (GGA)[45] and the projector augmented wave method (PAW)[46,47] as implemented in the Vienna ab initio simulation program (VASP).[48,49] For H and Li, all-electron PAW data sets were used, whereas for B and C the 1s core state was kept frozen. A kinetic energy cutoff of 550 eV was employed for the plane wave expansion of the Kohn–Sham orbitals.

Van der Waals interactions play an important role in the intercalation of Li into graphite. Such interactions are not included in a GGA functional such as PBE. To obtain a proper intercalation energy, we used the optB88-vdW functional, which contains the van der Waals density functional of Dion et al.[50] and the optB88 exchange term, and is implemented in VASP according to an efficient algorithm.[51,52] Details of the calculations of Li intercalation in graphite will be published elsewhere.[53]

The energies of nanoclusters were calculated in a periodically repeated cubic box which included at least 12 Å of vacuum in each direction to separate the periodic images. The energies of isolated H_2 and B_2H_6 molecules were calculated in cubic boxes with sizes of 12 and 14 Å, respectively. The ground-state geometries of the small clusters are described in detail in ref 34. The range of the interaction between the clusters and graphite is typically limited to the top graphite layers, so often we just use a single graphene layer to model this interaction. In the next section we discuss the accuracy of this approximation. The internal atomic positions were optimized with the conjugate gradient method until the forces on atoms were less than 0.01 eV/Å. This is sufficient to obtain converged total energies. For the nanocluster/graphene systems, a Γ-centered $3 \times 3 \times 1$ k-point mesh was used for the Brillouin zone integration, which is sufficiently accurate as the supercells are large (see the next section). The Methfessel–Paxton (MP)[54] scheme with a smearing width of 0.2 eV was employed for the occupation of the electronic levels.

To include the effects of the vibrational degrees of freedom on the calculated (free) energies, vibrational frequencies were calculated for some of the isolated clusters[55] using finite difference methods.[56] For computational details, see ref 34. We assume that the cluster vibrations are not appreciably affected by interaction with graphene or graphite and use the vibrational densities of states of free-standing clusters. In general, this is a good approximation because the cluster–graphene interaction is moderate, and only a few modes are affected by it. We calculate the free energies of the clusters from the DFT total energies and the vibrational densities of states,[57] where we assume that the clusters are immobilized by confinement in a porous material (so we neglect contributions due to translational and rotational degrees of freedom). The free energies of H_2 gas and B_2H_6 gas are taken from the literature, using a gas pressure of 1 bar.[58,59] To assess the changes of the Li phonon modes upon intercalation into graphite, we calculated the lattice vibrational frequencies of the bulk graphite, LiC_6, LiC_{12}, and Li metal. Upon Li intercalation, the in-plane C–C bond length is weakened, which leads to lower vibrational frequencies.

Note that small $(LiBH_4)_n$ clusters do not show phase transitions like bulk $LiBH_4$, i.e. the Gibbs free energy of a cluster is a smooth (i.e., differentiable) curve. For instance, a small cluster does not have a well-defined melting point, but the configuration space probed increases gradually as a function of temperature as higher lying energy regions of the (anharmonic) potential landscape become accessible. Here we use the harmonic approximation to approximate the potential landscape and neglect any anharmonic effects. The dominant contributions to the temperature dependence of the free-energy differences associated with $(LiBH_4)_n$ decomposition reactions come from the gases released in the reactions. This suggests that the errors in the free energies of the clusters, made by using the harmonic approximation, are relatively small.

3. RESULTS

3.1. $(Li)_n$, $(LiH)_n$, $(LiB)_n$, $(B)_n$, $(LiBH_4)_n$, and $Li_2B_nH_n$ ($n \leq 12$) Nanoclusters on the Graphene Surface. In this section

dx.doi.org/10.1021/jp410676b | J. Phys. Chem. C 2014, 118, 5102–5109

we study the interaction of the reactant clusters $(LiBH_4)_n$ and several possible product clusters with the graphene surface. In order to avoid spurious interactions between periodic images, we repeat the graphene unit cell eight times in both the *a* and *b* directions and use an 8 × 8 hexagonal in-plane supercell, which has a cell parameter of 19.74 Å and contains 128 C atoms. In the perpendicular (*c*) direction, the graphene layers are 20 Å apart. The binding energy of a nanocluster to the graphene surface is defined as

$$E_b^{nc} = E_{nc-gr} - E_{gr} - E_{nc} \quad (1)$$

where E_{nc-gr} and E_{gr} are the total energies of the graphene supercell with and without the nanocluster at the surface, respectively, and E_{nc} is the total energy of an isolated nanocluster. Note that a negative value for E_b^{nc} indicates a stable bond. In the following we use clusters with n = 1,4, and 12 formula units (f.u.) as examples.

The binding energies of the nanoclusters to single layer graphene are summarized in Table 1. For a single $LiBH_4$ molecule (n = 1) on the graphene surface, the most stable configuration has Li above the center of a C_6 hexagon (Figure 1). The binding energy of −0.246 eV is moderate. The Li−B bond length increases by a paltry 0.04 Å as compared to the that of the isolated $LiBH_4$ molecule. The calculated binding energy of $LiBH_4$ on C_{60} is −0.50 eV,[60,61] indicating that a curved graphene surface might lead to a somewhat stronger binding. Larger $(LiBH_4)_n$ clusters, such as $(LiBH_4)_4$ and $(LiBH_4)_{12}$ (see Figure 1), hardly bind to the graphene surface at all. They have negligible binding energies of −0.033 and −0.005 eV, respectively. This behavior is consistent with the binding being dominated by electrostatic forces, which is to be expected of clusters composed of ions (Li^+ and BH_4^-). A $(LiBH_4)_1$ molecule has a significant dipole moment, whose field induces a charge displacement in the (semimetallic) graphene sheet, and the Li^+ end of the molecule can approach the graphene sheet without steric hindrance. The larger clusters are more symmetric; the Li^+ ions are shielded by the BH_4^- ions, which decreases the local fields and prevents a close approach to the graphene surface.

Table 1. Calculated Binding Energies E_b^{nc} of $(LiH)_n$, $(LiB)_n$, $(B)_n$, $(LiBH_4)_n$, and $Li_2B_nH_n$ Nanoclusters to a Graphene Layer

nanocluster	E_b^{nc} (eV)	nanocluster	E_b^{nc} (eV)
$(LiBH_4)_1$	−0.246	$(LiH)_4$	−0.089
$(LiBH_4)_4$	−0.033	$(LiH)_{10}$	−0.109
$(LiBH_4)_{12}$	−0.005	$(LiH)_{12}$	−0.110
$Li_2B_4H_4$	−0.248	$Li_2B_{12}H_{12}$	−0.220
B_4	−0.521	$(LiB)_4$	−0.894
B_{12}	−0.058	$(LiB)_{12}$	−1.587

As for $(LiH)_n$ nanoclusters, which are possible decomposition products of the $(LiBH_4)_n$ clusters (see Section 3.2), the calculated binding energies to graphene are small, i.e., ∼−0.1 eV (Table 1). Again, these clusters consist of a rather symmetric stacking of oppositely charged ions (Li^+ and H^-), which leads to a rather moderate interaction with graphene. The $Li_2B_nH_n$ clusters contain a core consisting of a $B_nH_n^{2-}$ ion with two Li^+ ions bonded on the outside.[34] Both the $Li_2B_4H_4$ and the $Li_2B_{12}H_{12}$ clusters bind via a single Li ion to graphene, with moderate binding energies of −0.248 and −0.220 eV, respectively, consistent with electrostatic bonding. In contrast, the $(LiB)_n$ clusters have a much stronger binding to graphene. These clusters contain a B_n^{-n} core with n Li^+ ions bonded on the outside (Figure 1). This geometry makes the Li^+ ions easily accessible for electrostatic bonding to graphene. Indeed, all of the Li atoms in $(LiB)_4$ and multiple Li atoms in $(LiB)_{12}$ clusters bind to graphene, see Figure 1, with significant total binding energies of −0.894 and −1.587 eV, respectively.

The boron atoms in the B_n clusters considered here form covalent networks with a rather planar geometry,[34] which tend to interact with graphene only via B atoms on the edges of the network. The most stable configuration of the B_4 cluster has one boron atom on top of a carbon atom with a binding energy of −0.521 eV. The binding energy of B_{12} on graphene is −0.058 eV, i.e. it hardly interacts with graphene at all.

We will use the binding energies of clusters on graphene to study decompostion reactions of $(LiBH_4)_n$ clusters in Section 3.2. One may argue that clusters bonded to graphite (multilayer

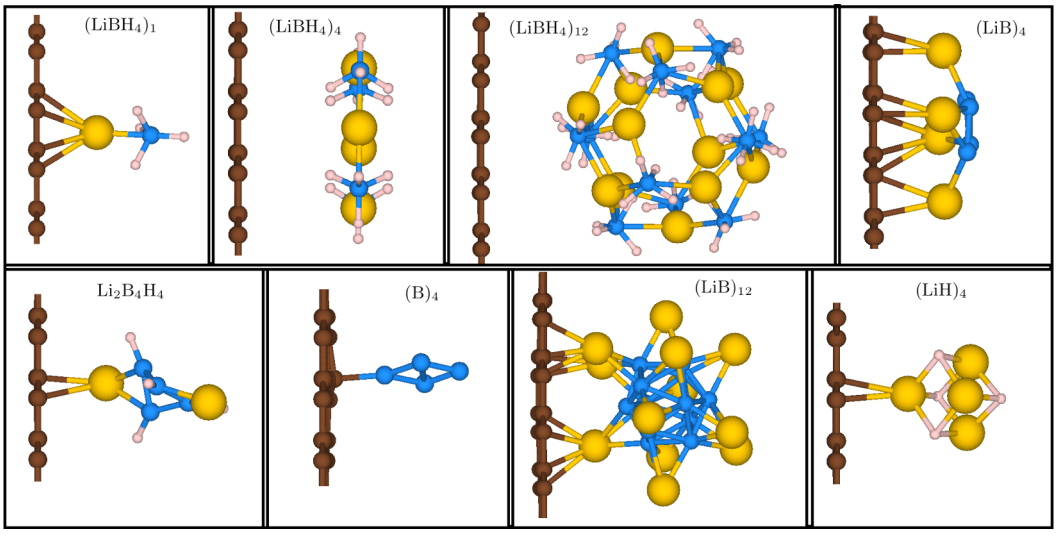

Figure 1. Optimized geometries of representative nanoclusters at the surface of a single graphene layer. The spheres represent Li (yellow), B (blue), H (pink), and C (brown) atoms.

dx.doi.org/10.1021/jp410676b | J. Phys. Chem. C 2014, 118, 5102−5109

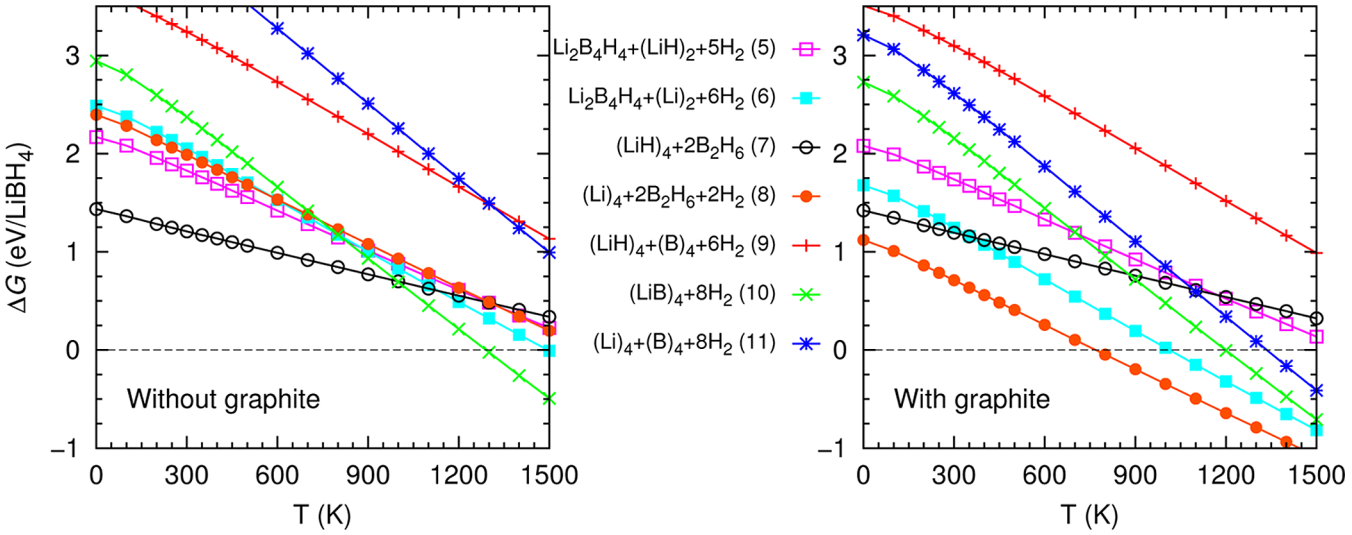

Figure 2. ΔG/f.u. of the $(LiBH_4)_4$ cluster as a function of temperature for various possible decomposition reactions without and in the presence of graphite. In the figure on the right (with graphite), reactions 6, 8, and 11 have Li intercalated into graphite, i.e. $(Li)_n \rightarrow n$ Li @ C_∞. Gas pressures are 1 bar.

graphene) would be better model systems. We approximate the binding to graphite by that to graphene and believe this to be a reasonable approximation. For a single Li atom we find a binding energy difference of ∼13% between binding to a single graphene sheet and to a graphite surface. A single Li atom donates most of its valence electron to graphene or graphite, and the difference in binding energy is caused mainly by a difference in electrostatic screening between the two substrates. Most of the binding energies in Table 1 are quite moderate, and an error of ∼13% would be tolerable in an absolute sense. Actually, the binding energies of $(LiBH_4)_n$, $(LiH)_n$, and $Li_2B_nH_n$ clusters are roughly independent of the size n or even decrease with increasing n, so any error made tends to decrease with increasing n, if counted per $LiBH_4$ unit (which we will do if we compare different reactions).

$(LiB)_n$ clusters might be a case where one might be more careful as they bind to graphene with a substantial energy. However, decomposition of $(LiBH_4)_n$ to $(LiB)_n$ turns out to be unfavorable with respect to other reaction paths. In order to have this decomposition reaction become competitive to other reactions, an increase of the binding of $(LiB)_n$ to the substrate of more than ∼1 eV per LiB is required. It is extremely unlikely to get such a stabilization by adding graphene layers.[62] The binding of B_n clusters is dictated by local covalent bonding to the (top) graphene layer where screening effects are of minor importance.

3.2. Decomposition of $(LiBH_4)_n$ Clusters. The decomposition of bulk $LiBH_4$ takes place at a high temperature ($T >$ 400 °C) and is proposed to proceed as[63,64]

$$LiBH_4 \leftrightarrow \frac{1}{12}Li_2B_{12}H_{12} + \frac{5}{6}LiH + \frac{13}{12}H_2(g) \quad (2)$$

$$\leftrightarrow LiH + B + \frac{3}{2}H_2(g) \quad (3)$$

After the first step we have $Li_2B_{12}H_{12}$ as an intermediate. Recently it has been argued that the first step is actually different and gives diborane (B_2H_6) as intermediate according to

$$LiBH_4 \leftrightarrow LiH + \frac{1}{2}B_2H_6(g) \quad (4)$$

Then, in a second step at $T >$ 250 °C, the diborane decomposes to B and H_2.[65] It is proposed that $Li_2B_{12}H_{12}$ and an amorphous $Li_2B_{10}H_{10}$ phase are formed only in a side reaction between diborane and the unreacted $LiBH_4$ at lower temperatures.

For the two basic bulk dehydrogenation reactions of $LiBH_4$, i.e., to $Li_2B_{12}H_{12}$ and LiH (reaction 2) and to B and LiH (reaction 3), we obtain energies of 0.39 and 0.84 eV/$LiBH_4$, respectively (at T = 0 K, including zero-point energies). These numbers are in good agreement with calculated values reported in the literature.[2,66−68]

3.2.1. Small Clusters. We select two cluster sizes $(LiBH_4)_n$ with n = 4 and n = 12. The latter can decompose into $Li_2B_{12}H_{12}$, which is the smallest cluster that contains a $(B_{12}H_{12})^{2-}$ ion. Such ions are the building blocks of bulk $Li_2B_{12}H_{12}$ [cf. reaction 2 above]. Hence, n = 12 forms a natural demarcation between small and large clusters. Very small clusters can behave very differently from bulk,[34] and we use n = 4 as an example of such a cluster. We consider the following possible decomposition reactions for $(LiBH_4)_n$ clusters

$$(LiBH_4)_n \leftrightarrow Li_2B_nH_n + (LiH)_{n-2} + (n+1)H_2(g) \quad (5)$$

$$(LiBH_4)_n \leftrightarrow Li_2B_nH_n + (Li)_{n-2} + \frac{3n}{2}H_2(g) \quad (6)$$

$$(LiBH_4)_n \leftrightarrow (LiH)_n + \frac{n}{2}B_2H_6(g) \quad (7)$$

$$(LiBH_4)_n \leftrightarrow (Li)_n + \frac{n}{2}B_2H_6(g) + \frac{n}{2}H_2(g) \quad (8)$$

$$(LiBH_4)_n \leftrightarrow (LiH)_n + (B)_n + \frac{3n}{2}H_2(g) \quad (9)$$

$$(LiBH_4)_n \leftrightarrow (LiB)_n + 2nH_2(g) \quad (10)$$

$$(LiBH_4)_n \leftrightarrow (Li)_n + (B)_n + 2nH_2(g) \quad (11)$$

We should mention that reaction 10 is unlikely to occur in bulk $LiBH_4$. Indeed, stoichiometric LiB is not known as a bulk compound. However, small clusters (e.g., of the sizes n = 4 and

dx.doi.org/10.1021/jp410676b | J. Phys. Chem. C 2014, 118, 5102−5109

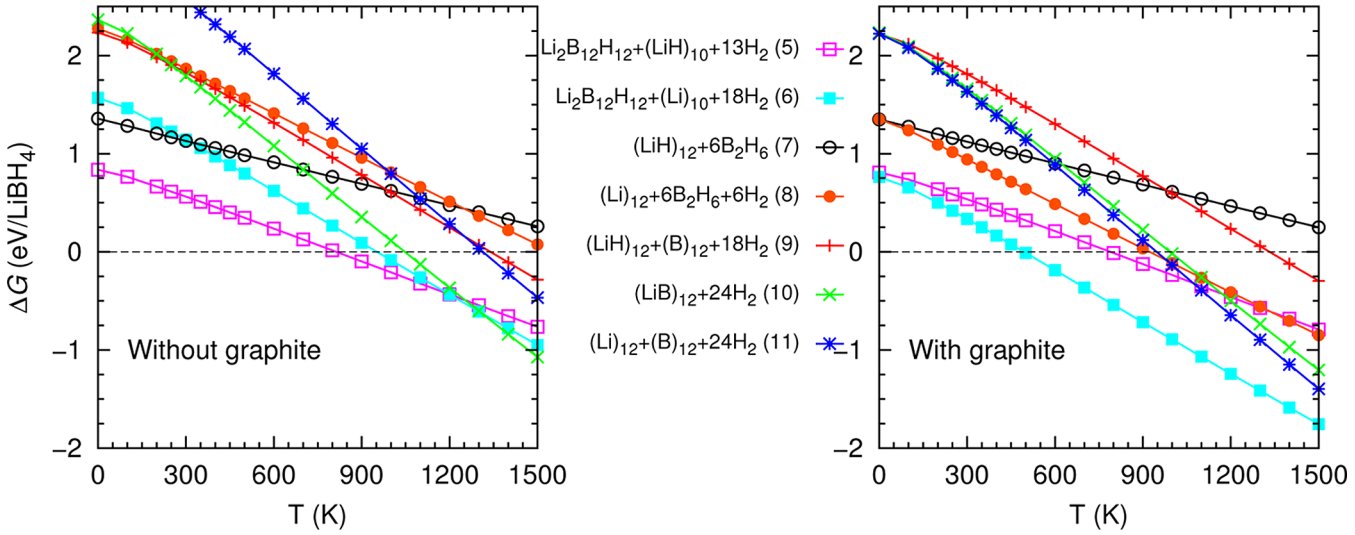

Figure 3. ΔG/$LiBH_4$ f.u. of $(LiBH_4)_{12}$ cluster as a function of temperature for different possible decomposition reactions without and with the presence of graphite. In the figure on the right (with graphite), reactions 6, 8 and 11 have Li intercalated into graphite, i.e. $(Li)_n \rightarrow n$ Li @ C_∞. Gas pressures are 1 bar.

n = 12 considered in this work) can behave very differently from bulk.[34] Note that reactions 5 and 6 are specific for $n \leq 12$, where a $(B_{12}H_{12})^{2-}$ cannot occur. Reaction 5 is the small-cluster replacement of reaction 2.

Reversible Li intercalation into the graphitic carbon host during dehydrogenation of nanoconfined $LiBH_4$ has been observed in experiment.[41,69] Our calculated intercalation energy is −1.85 eV/Li, which corresponds to intercalating a free Li atom in the compound LiC_{12}.[53,70] This means that Li intercalation in graphite has an enormous potential to stabilize the dehydrogenated state in reactions 6, 8, and 11. The stabilization is partially offset, of course, by the energy it costs to dissociate a $(Li)_n$ cluster. The net stabilization energy for n Li atoms result from

$$(Li)_n \rightarrow n\mathrm{Li}(^2S_{1/2}) \rightarrow n\mathrm{Li@C}_\infty \qquad (12)$$

The first step represents the (positive) dissociation energy of a $(Li)_n$ cluster, and the last step represents the (negative) intercalation energy of Li into graphite. The energy cost to dissociate a $(Li)_n$ cluster increases with increasing n, so the stabilization of the dehydrogenated state decreases with increasing n. We incorporate the stabilization energy in the energy balance of reactions 6, 8, and 11.

Figure 2 shows the change in free energy ΔG per formula unit of $LiBH_4$ as a function of temperature for the possible decomposition reactions 5−11 of the $(LiBH_4)_4$ (n = 4) cluster. It compares the reactions in vacuum to the reactions in the presence of a carbon host. Reactions that do not have Li as one of the products are hardly affected, i.e. reactions 5, 7, 9, and 10. Evidently the interactions of the reactant and product clusters with the carbon substrate have only a small net effect on the free-energy change of these reactions. In contrast, the effects for the three reactions that involve Li as a product are dramatic. The intercalation of Li into the carbon host shifts the ΔG curves pertaining to reactions 6, 8, and 11 down by 0.81, 1.27, and 1.40 eV, respectively.

Reaction equilibrium is achieved at the temperature T_d at which $\Delta G(T_d) = 0$. Without graphite, the small $(LiBH_4)_4$ cluster decomposes at a very high temperature $T_d \gtrsim 1300$ K. The dehydrogenation reaction to 10 $(LiB)_4$ is then most favorable. With graphite, all reactions leading to intercalated Li have a much lower ΔG. Indeed, reaction 8, leading to Li, B_2H_6(g), and H_2(g), has now become most favorable, with a decomposition temperature $T_d \approx 760$ K.

For the larger cluster $(LiBH_4)_{12}$ (n = 12), we observe a similar behavior (Figure 3). The reactions leading to intercalated Li are stabilized, whereas other reactions are hardly affected. Without graphite, the $(LiBH_4)_{12}$ cluster decomposes at $T_d \approx 800$ K. Most favorable is desorption reaction 5, where $Li_2B_{12}H_{12}$ and $(LiH)_{10}$ clusters are formed. Decomposition of the $(LiH)_{10}$ clusters takes place at much higher temperatures, $T_d \approx 1200$ K. Compared to the smaller cluster of Figure 2, reaction 10 to $(LiB)_n$ has become totally unimportant, as it outperforms the others only for temperatures $T > 1200$ K.

With graphite, the $(LiBH_4)_{12}$ cluster decomposes at a much lower temperature T_d = 490 K, according to reaction 6, where besides $Li_2B_{12}H_{12}$ clusters, (intercalated) Li and hydrogen are formed. Compared to the graphite-free case, the presence of graphite promotes the immediate decomposition of LiH clusters, thus releasing more hydrogen. In contrast to the case of n = 4, reaction 8, which releases B_2H_6 in addition to H_2, is not favorable. This means that from a thermodynamic point of view it is unlikely that B_2H_6 gas is formed in the decomposition of larger clusters. This is in agreement with recent experimental results on the desorption reaction of nanoconfined $LiBH_4$.[28]

3.2.2. Large Clusters. So far, we have considered the decomposition of $(LiBH_4)_n$ clusters with n = 4 and 12 by explicit calculations on these small clusters. Here we want to model the stabilizing effect of Li intercalation for clusters of a larger size. One can model the equilibrium shape of large nanoclusters from calculated surface energies using the Wulff theorem.[34,71] Once the shape of a nanocluster is determined, we calculate its total energy as

$$E_{\mathrm{cluster}}(n) = nE_{\mathrm{bulk}} + \sum_i \gamma_i A_i \qquad (13)$$

where γ_i is the surface energy of the ith nanocluster face and A_i is the area of the corresponding face. E_{bulk} is the bulk total energy per f.u. With this simple model one can calculate the H_2

dx.doi.org/10.1021/jp410676b | J. Phys. Chem. C 2014, 118, 5102−5109

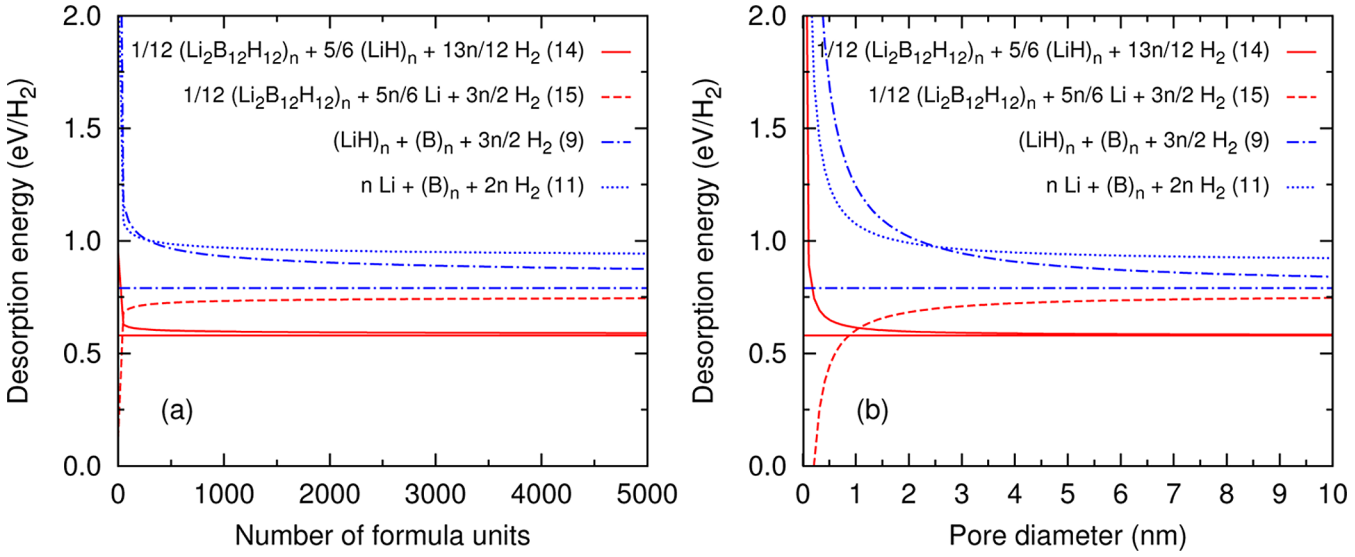

Figure 4. Calculated desorption energies as a function of (a) the number of formula units and (b) pore diameter. For reactions 11 and 15, the dehydrogenated state with Li intercalated into graphite is plotted. Horizontal lines are the corresponding bulk desorption energies.

desorption energy as a function of the cluster size n, provided n is sufficiently large.[72] Alternatively, one can calculate the H_2 desorption energy as a function of the size of the pores in the host material. For the latter we assume that the pores are spherical and of a fixed size and that each pore is filled with the largest possible crystallite of optimal shape of a single (reactant or product) compound.

We include the effect of the stabilization mechanism of reaction 12. So in reactions that would lead to a $(Li)_n$ cluster as a product, we assume that it dissociates immediately and the Li atoms intercalate into graphite. As $Li_2B_{12}H_{12}$ is a stable compound, we switch from reactions 5 and 6 to 14 and 15 for larger clusters,

$$(LiBH_4)_n \leftrightarrow \frac{1}{12}(Li_2B_{12}H_{12})_n + \frac{5}{6}(LiH)_n + \frac{13n}{12}H_2(g) \quad (14)$$

$$(LiBH_4)_n \leftrightarrow \frac{1}{12}(Li_2B_{12}H_{12})_n + \frac{5}{6}(Li)_n + \frac{3n}{2}H_2(g) \quad (15)$$

Figure 4 shows the desorption energies per H_2 released as a function of (a) n, the number of f.u., and (b) the pore diameter for the desorption reactions 14 and 9, which lead to $Li_2B_{12}H_{12}$ and B as a product, respectively, besides LiH. In addition, desorption energies of reactions 15 and 11 are shown, which also lead to $Li_2B_{12}H_{12}$ and B, but where LiH dissociates immediately into intercalated Li and hydrogen gas.

For large clusters, the stabilization due to Li intercalation is unable to push the desorption energy of the reaction with graphite below those of the reactions without graphite. The desorption energy of reaction 9 is lower than that of reaction 11, and that of 14 is lower than that of 15. Indeed, for large clusters, the desorption energy of reaction 9 drops with size faster than that of reaction 11, and the desorption energy of 15 even increases where that of 14 drops. So there is no apparent beneficial effect of Li intercalation, except maybe at a very high temperature, where decomposition of $LiBH_4$ into the elements, reaction 11, would be favored.

For small pore and cluster sizes, the situation is different. In the case in which the pores have a diameter $\lesssim$1.0 nm, Li intercalation leads to lower hydrogen desorption temperatures through reaction 15. For larger pore sizes, the beneficial effect on this particular reaction is lost. If we consider higher temperatures where other reactions become important, the effect of Li intercalation is operative for larger clusters and pores. For pore sizes $\lesssim$2.5 nm, reaction 11 is more favorable than 9. Indeed, the effect on the hydrogen desorption energy is 0.2 eV/H_2 for a 1.0 nm pore diameter. We should mention that these numbers are on the edge of what is reasonable using the Wulff construction. If the cluster size $n \lesssim 40$ f.u. or the pore diameter $\lesssim$1.0 nm, one should use calculations on explicit clusters as in Section 3.2.1.

4. SUMMARY

Recent experimental studies suggest that $LiBH_4$ nanoparticles confined in nanoporous carbon materials show faster desorption kinetics and improved reversibility as compared to those of bulk $LiBH_4$, and even could have more favorable thermodynamics. However, calculations on isolated $LiBH_4$ nanoclusters show that the reaction energies of such clusters are very close to that of bulk, if the cluster diameter $\gtrsim$2 nm, and even become more unfavorable if the diameter $\lesssim$1 nm.[34] This opens up the question whether the thermodynamics of the dehydrogenation reactions might be altered by chemical interactions between the reactant and products and the nanoporous carbon host material. In this work we address the latter by studying the interaction of the reactant and product clusters with graphene and graphite and by evaluating the role of reversible intercalation of Li (one of the possible reaction products) into graphite.

DFT calculations on small $(LiBH_4)_n$, n = 4 and 12, clusters adsorbed on graphene show that reaction energies are not very sensitive to the interaction of these nanoclusters and the carbon surface. Our findings show that intercalation of Li plays a more important role and has a large potential to stabilize the dehydrogenated state of reactions where a $(Li)_n$ cluster is one of the products. By dissociating such clusters and intercalating the resulting Li atoms into the carbon material, we can alter the reaction pathways and obtain considerably lower decomposition temperatures for small $(LiBH_4)_n$ clusters. For instance, the

dx.doi.org/10.1021/jp410676b | J. Phys. Chem. C 2014, 118, 5102−5109

calculated decomposition temperature $T_d \approx 800$ K of $(LiBH_4)_{12}$ to $Li_2B_{12}H_{12}$, LiH, and H_2 drops to $T_d \approx 500$ K because LiH decomposes immediately to Li and H_2, and Li is intercalated.

For larger $(LiBH_4)_n$ clusters, the Li intercalation effect in stabilizing the dehydrogenated state becomes much smaller. This is partly due to the fact that it costs more energy to break up larger Li clusters; the net energy gain due to intercalation saturates at the value of −0.2 eV/Li with respect to Li bulk. Moreover, as the stability of the $(LiH)_n$ clusters increases with size, the dehydrogenated state with $(LiH)_n$ and not $(Li)_n$ clusters becomes more favorable for larger $(LiBH_4)_n$ clusters.

In conclusion, Li intercalation into graphitic structures is important in stabilizing the dehydrogenated state in nanoclusters. It allows for H that is trapped in LiH to be released. However, only for small clusters can it tip the thermodynamic balance in favor of this mechanism and reduce the desorption temperature.

AUTHOR INFORMATION

Corresponding Authors

*E-mail: e.hazrati@science.ru.nl. Phone: +31 (0)243652984. Fax: +31 (0)243652120.

*E-mail: g.dewijs@science.ru.nl. Phone: +31 (0)243652984. Fax: +31 (0)243652120.

Notes

The authors declare no competing financial interest.

ACKNOWLEDGMENTS

The authors thank Petra de Jongh and Peter Ngene for useful discussions. The work of E.H. is part of the Sustainable Hydrogen program of Advanced Chemical Technologies for Sustainability (ACTS), Project 053.61.019. The work of G.A.W. is part of the research program of the Foundation for Fundamental Research on Matter (FOM), which is part of The Netherlands Organisation for Scientific Research (NWO).

REFERENCES

(1) Schlapbach, L.; Züttel, A. Hydrogen-Storage Materials for Mobile Applications. *Nature* **2001**, *414*, 353−358.

(2) van Setten, M. J.; de Wijs, G. A.; Fichtner, M.; Brocks, G. A Density Functional Study of α-$Mg(BH_4)_2$. *Chem. Mater.* **2008**, *20*, 4952−4956.

(3) Er, S.; de Wijs, G. A.; Brocks, G. Tuning the Hydrogen Storage in Magnesium Alloys. *J. Phys. Chem. Lett.* **2010**, *1*, 1982−1986.

(4) Züttel, A.; Wenger, P.; Rentsch, S.; Sudan, P.; Mauron, P.; Emmenegger, C. $LiBH_4$ a New Hydrogen Storage Material. *J. Power Sources* **2003**, *118*, 1−7.

(5) Orimo, S.-I.; Nakamori, Y.; Eliseo, J.; Züttel, A.; Jensen, C. Complex Hydrides for Hydrogen Storage. *Chem. Rev.* **2007**, *107*, 4111−4132.

(6) Züttel, A.; Borgschulte, A.; Orimo, S.-I. Tetrahydroborates as New Hydrogen Storage Materials. *Scr. Mater.* **2007**, *56*, 823−828.

(7) Sakintuna, B.; Lamaridarkrim, F.; Hirscher, M. Metal Hydride Materials for Solid Hydrogen Storage: A Review. *Int. J. Hydrogen Energy* **2007**, *32*, 1121−1140.

(8) George, L.; Saxena, S. Structural Stability of Metal Hydrides, Alanates and Borohydrides of Alkali and Alkali-earth Elements: A Review. *Int. J. Hydrogen Energy* **2010**, *35*, 5454−5470.

(9) Jain, I.; Jain, P. Novel Hydrogen Storage Materials: A Review of Lightweight Complex Hydrides. *J. Alloys Compd.* **2010**, *503*, 303−339.

(10) Yang, J.; Hirano, S. Improving the Hydrogen Reaction Kinetics of Complex Hydrides. *Adv. Mater.* **2009**, *21*, 3023−3028.

(11) de Jongh, P. E.; Adelhelm, P. Nanosizing and Nanoconfinement: New Strategies Towards Meeting Hydrogen Storage Goals. *ChemSusChem* **2010**, *3*, 1−18.

(12) Au, M.; Walters, R. T. Reversibility Aspect of Lithium Borohydrides. *Int. J. Hydrogen Energy* **2010**, *35*, 10311−10316.

(13) Gutowska, A.; Li, L.; Shin, Y.; Wang, C. M.; Li, X. S.; Linehan, J. C.; Smith, R. S.; Kay, B. D.; Schmid, B.; Shaw, W.; et al. Nanoscaffold Mediates Hydrogen Release and the Reactivity of Ammonia Borane. *Angew. Chem., Int. Ed.* **2005**, *44*, 3578−3582.

(14) de Jongh, P. E.; Adelhelm, P. Nanosizing and Nanoconfinement: New Strategies Towards Meeting Hydrogen Storage Goals. *ChemSusChem* **2010**, *3*, 1332−1348.

(15) Adelhelm, P.; de Jongh, P. E. The Impact of Carbon Materials on the Hydrogen Storage Properties of Light Metal Hydrides. *J. Mater. Chem.* **2011**, *21*, 2417−2427.

(16) Gao, J.; Adelhelm, P.; Verkuijlen, M. H. W.; Rongeat, C.; Herrich, M.; van Bentum, P. J. M.; Gutfleisch, O.; Kentgens, A. P. M.; de Jong, K. P.; de Jongh, P. E. Confinement of $NaAlH_4$ in Nanoporous Carbon: Impact on H_2 Release, Reversibility, and Thermodynamics. *J. Phys. Chem. C* **2010**, *114*, 4675−4682.

(17) Lohstroh, W.; Roth, A.; Hahn, H.; Fichtner, M. Thermodynamic Effects in Nanoscale $NaAlH_4$. *ChemPhysChem* **2010**, *11*, 789−792.

(18) Mueller, T.; Ceder, G. Effect of Particle Size on Hydrogen Release from Sodium Alanate Nanoparticles. *ACS Nano* **2010**, *4*, 5647−5656.

(19) Majzoub, E. H.; Zhou, F.; Ozoliņš, V. First-Principles Calculated Phase Diagram for Nanoclusters in the Na−Al−H System: A Single-Step Decomposition Pathway for $NaAlH_4$. *J. Phys. Chem. C* **2011**, *115*, 2636−2643.

(20) Vajo, J.; Salguero, T.; Gross, a.; Skeith, S.; Olson, G. Thermodynamic Destabilization and Reaction Kinetics in Light Metal Hydride Systems. *J. Alloy. Compd.* **2007**, *446*−*447*, 409−414.

(21) Gross, A. F.; Vajo, J. J.; Van Atta, S. L.; Olson, G. L. Enhanced Hydrogen Storage Kinetics of $LiBH_4$ in Nanoporous Carbon Scaffolds. *J. Phys. Chem. C* **2008**, *112*, 5651−5657.

(22) Fang, Z.; Wang, P.; Rufford, T.; Kang, X.; Lu, G.; Cheng, H. Kinetic- and Thermodynamic-Based Improvements of Lithium Borohydride Incorporated into Activated Carbon. *Acta Mater.* **2008**, *56*, 6257−6263.

(23) Cahen, S.; Eymery, J.-B.; Janot, R.; Tarascon, J.-M. Improvement of the $LiBH_4$ Hydrogen Desorption by Inclusion into Mesoporous Carbons. *J. Power Sources* **2009**, *189*, 902−908.

(24) Ngene, P.; Adelhelm, P.; Beale, A. M.; de Jong, K. P.; de Jongh, P. E. $LiBH_4$/SBA-15 Nanocomposites Prepared by Melt Infiltration under Hydrogen Pressure: Synthesis and Hydrogen Sorption Properties. *J. Phys. Chem. C* **2010**, *114*, 6163−6168.

(25) Ngene, P.; van Zwienen, R.; de Jongh, P. E. Reversibility of the Hydrogen Desorption from $LiBH_4$: A Synergetic Effect of Nanoconfinement and Ni Addition. *Chem. Commun.* **2010**, *46*, 8201−8203.

(26) Shane, D. T.; Corey, R. L.; McIntosh, C.; Rayhel, L. H.; Bowman, R. C.; Vajo, J. J.; Gross, A. F.; Conradi, M. S. $LiBH_4$ in Carbon Aerogel Nanoscaffolds: An NMR Study of Atomic Motions. *J. Phys. Chem. C* **2010**, *114*, 4008−4014.

(27) Liu, X.; Peaslee, D.; Jost, C. Z.; Majzoub, E. H. Controlling the Decomposition Pathway of $LiBH_4$ via Confinement in Highly Ordered Nanoporous Carbon. *J. Phys. Chem. C* **2010**, *114*, 14036−14041.

(28) Liu, X.; Peaslee, D.; Jost, C. Z.; Baumann, T. F.; Majzoub, E. H. Systematic Pore-Size Effects of Nanoconfinement of $LiBH_4$: Elimination of Diborane Release and Tunable Behavior for Hydrogen Storage Applications. *Chem. Mater.* **2011**, *23*, 1331−1336.

(29) Sun, W.; Li, S.; Mao, J.; Guo, Z.; Liu, H.; Dou, S.; Yu, X. Nanoconfinement of Lithium Borohydride in Cu-MOFs Towards Low Temperature Dehydrogenation. *Dalton Trans.* **2011**, *40*, 5673−5676.

(30) Ngene, P.; Verkuijlen, M. H. W.; Zheng, Q.; Kragten, J.; van Bentum, P. J. M.; Bitter, J. H.; de Jongh, P. E. The Role of Ni in Increasing the Reversibility of the Hydrogen Release from Nanoconfined $LiBH_4$. *Faraday Discuss.* **2011**, *151*, 47−58.

(31) Ngene, P. *Nanoconfined Alkali-Metal Borohydrides for Reversible Hydrogen Storage*. Ph.D. Thesis, Utrecht University, Utrecht, The Netherlands, 2012.
(32) Hazrati, E.; Brocks, G.; Buurman, B.; de Groot, R. A.; de Wijs, G. A. Intrinsic Defects and Dopants in $LiNH_2$: A First-Principles Study. *Phys. Chem. Chem. Phys.* **2011**, *13*, 6043−6052.
(33) Çakr, D.; de Wijs, G. A.; Brocks, G. Native Defects and the Dehydrogenation of $NaBH_4$. *J. Phys. Chem. C* **2011**, *115*, 24429−24434.
(34) Hazrati, E.; Brocks, G.; de Wijs, G. A. First-Principles Study of $LiBH_4$ Nanoclusters and Their Hydrogen Storage Properties. *J. Phys. Chem. C* **2012**, *116*, 18038−18047.
(35) Adelhelm, P.; de Jong, K. P.; de Jongh, P. E. How Intimate Contact with Nanoporous Carbon Benefits the Reversible Hydrogen Desorption from NaH and $NaAlH_4$. *Chem. Commun.* **2009**, 6261−6263.
(36) Joncourt, L.; Mermoux, M.; Touzain, P.; Bonnetain, L.; Dumas, D.; Allard, B. Sodium Reactivity with Carbons. *J. Phys. Chem. Solids* **1996**, *57*, 877−882.
(37) Dahn, J. R.; Zheng, T.; Liu, Y.; Xue, J. S. Mechanisms for Lithium Insertion in Carbonaceous Materials. *Science* **1995**, *270*, 590−593.
(38) Winter, M.; Besenhard, J. O.; Spahr, M. E.; Novák, P. Insertion Electrode Materials for Rechargeable Lithium Batteries. *Adv. Mater.* **1998**, *10*, 725−763.
(39) Er, S.; de Wijs, G. A.; Brocks, G. Hydrogen Storage by Polylithiated Molecules and Nanostructures. *J. Phys. Chem. C* **2009**, *113*, 8997−9002.
(40) Mandeltort, L.; Yates, J. T. Rapid Atomic Li Surface Diffusion and Intercalation on Graphite: A Surface Science Study. *J. Phys. Chem. C* **2012**, *116*, 24962−24967.
(41) Miedema, P. S.; Ngene, P.; van der Eerden, A. M. J.; Weng, T.-C.; Nordlund, D.; Sokaras, D.; Alonso-Mori, R.; Juhin, A.; de Jongh, P. E.; de Groot, F. M. F. In situ X-ray Raman Spectroscopy of $LiBH_4$. *Phys. Chem. Chem. Phys.* **2012**, *14*, 5581−5587.
(42) By using graphite we assume that the number of unsaturated reactive carbon sites is small. Such sites might otherwise lead to (poly) lithiated species, see ref 39.
(43) Hohenberg, P.; Kohn, W. Inhomogeneous Electron Gas. *Phys. Rev.* **1964**, *136*, B864.
(44) Kohn, W.; Sham, L. J. Self-Consistent Equations Including Exchange and Correlation Effects. *Phys. Rev.* **1965**, *140*, A1133.
(45) Perdew, J. P.; Burke, K.; Ernzerhof, M. Generalized Gradient Approximation Made Simple. *Phys. Rev. Lett.* **1996**, *77*, 3865−3868.
(46) Blöchl, P. Projector Augmented-wave Method. *Phys. Rev. B* **1994**, *44*, 13063−17979.
(47) Kresse, G.; Joubert, D. From Ultrasoft Pseudopotentials to the Projector Augmented-Wave Method. *Phys. Rev. B* **1999**, *59*, 1758−1775.
(48) Kresse, G.; Furthmüller, J. Efficient Iterative Schemes for Ab initio Total-Energy Calculations Using a Plane-Wave Basis Set. *Phys. Rev. B* **1996**, *54*, 11169−11186.
(49) Kresse, G.; Furthmüller, J. Efficiency of Ab-initio Total Energy Calculations for Metals and Semiconductors Using a Plane-wave Basis Set. *Comput. Mater. Sci.* **1996**, *6*, 15−50.
(50) Dion, M.; Rydberg, H.; Schröder, E.; Langreth, D. C.; Lundqvist, B. I. Van der Waals Density Functional for General Geometries. *Phys. Rev. Lett.* **2004**, *92*, 246401.
(51) Klimeš, J.; Bowler, D. R.; Michaelides, A. Van der Waals Density Functionals Applied to Solids. *Phys. Rev. B* **2011**, *83*, 195131.
(52) Román-Pérez, G.; Soler, J. M. Efficient Implementation of a van der Waals Density Functional: Application to Double-Wall Carbon Nanotubes. *Phys. Rev. Lett.* **2009**, *103*, 096102.
(53) Hazrati, E.; Brocks, G.; de Wijs, G. A. Li Intercalation in Graphite: A van der Waals Density Functional Study. To be submitted for publication..
(54) Methfessel, M.; Paxton, A. T. High-precision Sampling for Brillouin-zone Integration in Metals. *Phys. Rev. B* **1989**, *40*, 3616−3621.
(55) We calculate the zero-point vibrational energies and the temperature-dependent vibrational enthalpies and entropies of $Li_2B_nH_n$ (n = 4,12), $(LiBH_4)_{12}$, and $(LiB)_{12}$ clusters, explicitly. For Li_n, $(LiH)_n$, and B_n clusters with n = 4 and 12, the corresponding bulk values per f.u. are used. The calculated values for $(LiB)_{12}$ and $(LiBH_4)_{12}$ clusters per f.u. are used for $(LiB)_4$ and $(LiBH_4)_4$, respectively.
(56) Kresse, G.; Furthmüller, J.; Hafner, J. Ab initio Force Constant Approach to Phonon Dispersion Relations of Diamond and Graphite. *Europhys. Lett.* **1995**, *32*, 729−734.
(57) van Setten, M. J.; de Wijs, G. A.; Brocks, G. First-principles Calculations of the Crystal Structure, Electronic Structure, and Thermodynamic Stability of $Be(BH_4)_2$. *Phys. Rev. B* **2008**, *77*, 165115.
(58) Chase, M. W. *NIST-JANAF Thermochemical Tables*, 4th ed.; American Institute of Physics: Washington, DC,1998.
(59) The free energy is calculated as the sum of the total energy, ZPE and experimental data from the NIST-JANAF Thermochemical Tables.
(60) Scheicher, R. H.; Li, S.; Araujo, C. M.; Blomqvist, A.; Ahuja, R.; Jena, P. Theoretical Study of C_{60} as Catalyst for Dehydrogenation in $LiBH_4$. *Nanotechnology* **2011**, *22*, 335401.
(61) Energy calculated with PW91 GGA functional.
(62) By using graphite and including van der Waals interactions, we obtained a ∼ 0.25 eV/LiB higher binding energy.
(63) Orimo, S.-I.; Nakamori, Y.; Ohba, N.; Miwa, K.; Aoki, M.; Towata, S.-i.; Züttel, A. Experimental Studies on Intermediate Compound of $LiBH_4$. *Appl. Phys. Lett.* **2006**, *89*, 021920.
(64) Hwang, S.-J.; Bowman, R.; Reiter, J.; Rijssenbeek, J.; Soloveichik, G.; Zhao, J.-C.; Kabbour, H.; Ahn, C. NMR Confirmation for Formation of $[B_{12}H_{12}]^{2-}$ Complexes during Hydrogen Desorption from Metal Borohydrides. *J. Phys. Chem. C* **2008**, *112*, 3164−3169.
(65) Friedrichs, O.; Remhof, A.; Hwang, S.-J.; Züttel, A. Role of $Li_2B_{12}H_{12}$ for the Formation and Decomposition of $LiBH_4$. *Chem. Mater.* **2010**, *22*, 3265−3268.
(66) Miwa, K.; Ohba, N.; Towata, S.-I.; Nakamori, Y.; Orimo, S.-I. First-Principles Study on Lithium Borohydride $LiBH_4$. *Phys. Rev. B* **2004**, *69*, 245120.
(67) Siegel, D. J.; Wolverton, C.; Ozoliņš, V. Thermodynamic Guidelines for the Prediction of Hydrogen Storage Reactions and Their Application to Destabilized Hydride Mixtures. *Phys. Rev. B* **2007**, *76*, 134102.
(68) Ozolins, V.; Majzoub, E. H.; Wolverton, C. First-Principles Prediction of Thermodynamically Reversible Hydrogen Storage Reactions in the Li-Mg-Ca-B-H System. *J. Am. Chem. Soc.* **2009**, *131*, 230−237.
(69) Ngene, P.; Verkuijlen, M. H. W.; Zheng, Q.; Kragten, J.; van Bentum, P. J. M.; Bitter, J. H.; de Jongh, P. E. The Role of Ni in Increasing the Reversibility of the Hydrogen Release from Nano-confined $LiBH_4$. *Faraday Discuss.* **2011**, *151*, 47−58.
(70) We assume there is sufficient Li and sufficient C so that bulk LiC_{12} is formed, with possibly a remainder of bulk C.
(71) Wulff, G. On the Question of the Rate of Growth and Dissolution of Crystal Surfaces. *Z. Kristallogr.* **1901**, *34*, 449−530.
(72) A test calculation on a $(LiBH_4)_n$ n = 56 cluster showed that the Wulff construction is sufficiently accurate for clusters with size $n \gtrsim 56$. The total energy that is predicted by eq 13 becomes unreasonable, however, for $n < 40$.